Numerical Modeling of the Transient Chilldown Process of a Cryogenic Propellant Transfer Line

Jason Hartwig[1] and Jerry Vera[2]
NASA Glenn Research Center, Cleveland, OH, 44135, USA

Before cryogenic fuel depots can be fully realized, efficient methods with which to chill down the spacecraft transfer line and receiver tank are required. This paper presents numerical modeling of the chilldown of a liquid hydrogen tank-to-tank propellant transfer line using the Generalized Fluid System Simulation Program (GFSSP). To compare with data from recently concluded turbulent LH_2 chill down experiments, seven different cases were run across a range of inlet liquid temperatures and mass flow rates. Both trickle and pulse chill down methods were simulated. The GFSSP model qualitatively matches external skin mounted temperature readings, but large differences are shown between measured and predicted internal stream temperatures. Discrepancies are attributed to the simplified model correlation used to compute two-phase flow boiling heat transfer. Flow visualization from testing shows that the initial bottoming out of skin mounted sensors corresponds to annular flow, but that considerable time is required for the stream sensor to achieve steady state as the system moves through annular, churn, and bubbly flow. The GFSSP model does adequately well in tracking trends in the data but further work is needed to refine the two-phase flow modeling to better match observed test data.

Nomenclature

C_p	=	Specific heat [J/kg*K]
DC	=	Duty Cycle [dimensionless]
k	=	Thermal conductivity [W/m*K]
t_{closed}	=	Valve-off time [s]
t_{open}	=	Valve-on time [s]
Nu	=	Nusselt number
Pr	=	Prandtl number
Re	=	Reynolds number
u	=	Fluid velocity [m/s]
μ	=	Viscosity [Pa*s]
ρ	=	Density [kg/m^3]
x	=	Quality
Y	=	Mass fraction

I. Introduction and Background

A fuel depot is defined as an Earth-orbiting storage vessel in Low Earth Orbit (LEO) used to store cryogenic propellant indefinitely so that customer spacecraft can rendezvous, dock, and extract the propellant en route to destinations far outside LEO. The depot would use cryogenic fluid management (CFM) technology to supply liquid to the vehicle storage tank to first chill down and then refill the propellant tank. This process is analogous to refueling an automobile at a gas station on the ground. Large fuel depots can therefore contain a large percentage of the propellant required for a deep space mission, thus allowing more dry mass launched into orbit. Due to its size, a fuel depot will likely need to be launched in stages and assembled in LEO. The initial cost of assembly will quickly be

[1]Research Aerospace Engineer, Propellants and Propulsion Branch, 21000 Brookpark Road, MS 301-3, Cleveland, Brookpark, OH 44142, and AIAA Senior Member.
[2]Aerospace Engineer, Fluids System Branch, 21000 Brookpark Road, MS 301-3, Cleveland, Brookpark, OH 44142.

outweighed by the long term, continuous usage of the fuel depot for routine commercial space flight. High performance in-space cryogenic engines coupled with large amounts of propellants equates to significantly higher Earth departure velocities and/or much longer duration missions beyond LEO. The lower overall cost, less risk, and fewer uncertainties in design and operation render the cryogenic fuel depot the primary candidate for enabling future long-duration missions. Example concepts of fuel depots exist in the literature (e.g. Chandler et al. 2007).

The current cost to launch and store cryogenic propellant in LEO is estimated at over $10,000 per kilogram of propellant. Therefore, before cryogenic fuel depots are fully realizable, efficient methods with which to chill down the customer spacecraft propellant transfer line and receiver tank are first required. Efficient methods to extract propellant from the depot storage tank (Hartwig 2014), to chill (Keefer 2010), and fill (Taylor and Chato 1991 and Wang et al. 2008) the receiver tank have been investigated previously.

Meanwhile very little work has been done to analytically or numerically characterize the transfer line chilldown process, though there have been a number of experimental studies on the flow physics associated with cryogenic transfer line chill down, see for example Glahn (1964), Kawanami et al. (2007a and b), Hu et al. (2012). Only one known experimental study on LH_2 transfer line chill down was conducted previously in Brennan et al. (1966). Cryogenic fluid flow, coupled with large temperature gradients between ambient and fluid implies that there will be complex two-phase flow boiling and heat transfer between wall and fluid. When working with liquid hydrogen (LH_2), problems are further exacerbated due to the low normal boiling point, low surface tension, and low density relative to other cryogenic fluids. Transfer lines for the proposed cryogenic depots are typically characterized by small diameter, long lines, with flow rates much smaller than those seen in engine line chill down (Schuster et al. 1996). Due to the projected cost to launch and store propellant in LEO, chilldown will be optimized to conserve mass.

Recently, LH_2 transfer line chilldown tests at high Reynolds numbers were conducted at NASA Glenn Research Center in Cleveland, OH. The purpose of the tests was to examine the efficiency of several different chilldown methods, to quantify the dynamic response of the system through the use of temperature, pressure, and flow visualization data, and to provide insight into the optimal design and operation of future depot transfer lines. The preliminary experimental results are reported in Rame et al. (2014). With new experimental data, it is highly desired to create numerical models that can be used to design and analyze future depot transfer systems. It is thus the purpose of the current paper to numerically model the recent LH_2 chilldown experiments and to assess the reliability of the model by comparing it with the data.

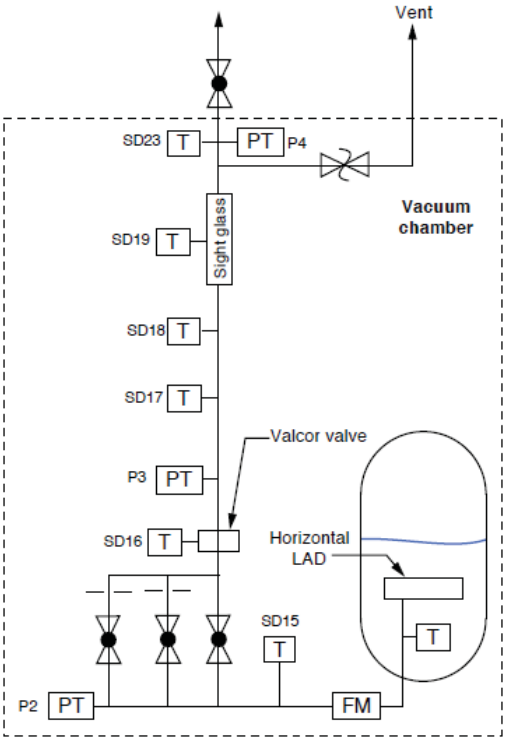

Figure 1: Schematic of Transfer Line Chilldown Test Hardware

II. Description of Hardware and Experiment

A schematic of the test hardware used for the LH_2 transfer line chilldown experiments is shown in Figure 1. A 3D model of the test hardware is depicted in Figure 2. Tests were performed at the Small Multi-Purpose Research Facility (SMiRF) at NASA GRC. Chilldown tests were performed over a wide range of liquid inlet temperatures (20.3 – 24.2K) and mass flow rates (0.0023 – 0.036 kg/s) using several different direct chilldown methods. A large storage dewar was used to house and condition liquid to the desired initial saturation temperature at the inlet of the transfer line. LH_2 was routed out of the bottom of the tank to the lowest portion of the vacuum chamber (VC) directly through a liquid flow meter. Flow was then routed to a flow control manifold. For the low and medium flow legs, flow was controlled through an isolation valve and orifice; for the high flow leg, the limiting flow restriction was the isolation valve itself. A second "dummy" valve was included to add mass to the transfer line. Flow was then routed vertically upward to simulate the axisymmetric heat input into the tube as in the microgravity case (Kawanami et al. 2007a). Fluid then entered a sight glass (SG) for two phase flow visualization as the chilldown process evolved. Flow was finally routed up through the VC lid, through a

heat exchanger, and then to the vent stack located outside SMiRF. The outer diameter of the tube was 1.27 cm (0.5 in).

The see-through portion of the SG was made of Pyrex glass. A protective can was mounted around the outside to reduce thermal stresses on the SG as shown in Figure 2. A flexible bellows piece was mounted between glass and steel portions of the line as shown on the right side of Figure 2. The flow was visualized through the use of a high speed camera, a backlit light source, and a high speed video data acquisition system to correlate between temperature and pressure data and visual imagery as a function of time.

Figure 2: Three-Dimensional Model of the Transfer Line Chilldown Test Hardware

The completed storage dewar, line chill assembly, and flow visualization system were attached to a vacuum chamber lid as shown in Figure 2. The whole assembly was then mounted inside a VC, which was held to a low back pressure of 1.33×10^{-7} kPa. The VC used a cryoshroud to set a reduced ambient temperature of 250K to simulate a cold solar inertial orbit of LEO. The mass and length of the warm section of the transfer line, which includes the two valves, orifice, piping, SG, and SG housing was approximately 3.42 kg and 1.61m, respectively.

Critical instrumentation is shown in Figures 1 and 2. Silicon diodes (SDs) were used to measure external skin temperatures as well as internal stream temperatures at various locations. Skin temperatures were taken at four locations, one measurement on the valve body (SD16), two measurements on the SS pipe (SD17 and SD18), and one on the Pyrex SG (SD19). Meanwhile, stream temperatures were taken inside the storage dewar, upstream of the flow control valve manifold, and downstream of the sight glass. Pressure was measured inside the storage dewar, upstream of the valve manifold, and up and downstream of the SG. Heaters were mounted on the line chill assembly to expedite the initial 250K boundary condition so that the next test could commence.

The following is the test sequence for conducting a line chill down experiment: Prior to testing, the cryoshroud was set to 250K, the test tank filled with LH_2, and the desired liquid saturation temperature and total tank pressure were achieved. Gaseous helium was used to pressurize the tank and achieve the desired level of subcooling. To conduct the test, the desired chill method and flow rate was chosen, and the testing proceeded until the system achieved a steady state condition. Steady state was taken at the point in time when the stream temperature downstream of the SG (SD23) was lower than the saturation temperature based on the local pressure downstream of the SG. Visually, this corresponded to bubbly flow ($x = 0.001$). Experimentally, this corresponded to fluctuations in temperature less than the uncertainty in the measurement (< 0.1K). The most stringent steady state criteria would have been subcooled liquid at the end of the transfer line, but flow visualization indicated that certain runs (especially at lower flow rates) did not achieve this strict criteria. After testing, the line heaters were engaged to warm the lines back to 250K, and then testing was repeated at the next desired condition.

III. Numerical Model

The Generalized Fluid System Simulation Program (GFSSP) was used to model the dynamic LH_2 transfer line chilldown process. GFSSP was originally formulated to model heat transfer and fluid flow in the Shuttle turbo machinery (Majumdar and Van Hooser 1995 and Schallhorn et al. 1998) and has also been applied to cryogenic feed systems (Richards and Vonderwall 1997), tank pressurization (Majumdar and Steadman 1999), Shuttle propellant loading (LeClair and Majumdar 2010), and no vent fill operation (Majumdar 2013). The code has since been updated to include modeling of chemical reactions (Sozen and Majumdar 2003) and conjugate heat transfer (Majumdar 2004).

A detailed description of the GFSSP code is available online; only general details are presented here. GFSSP is a general fluid flow system solver that allows users to calculate the velocities, pressures, and temperatures of liquids and gases inside fluid networks using a finite volume model of nodes and flow branches. It has the capability to model phase change, compressibility, mixture thermodynamics, and transient operations. At each fluid node, the conservation of mass, energy, and species concentration are solved to obtain the pressure, temperature, and concentration at that node. The programs GASP, WASP, and GASPAK are included in GFSSP to calculate thermodynamic and thermo-physical properties of selected fluids including liquid-vapor (saturation) conditions and vapor region. While these property tables are able to calculate mass fractions, it does not explicitly distinguish between droplet flow, annular flow, bubbly flow, or any other such physical description of the two-phase regime.

Pipe or tube materials are modeled using separate solid nodes of specified materials. These solid nodes connect to adjacent fluid nodes using network connections that calculate convective heat transfer at each distinct location. At each solid node, the energy conservation equation is solved to calculate the temperature of the solid. To calculate the convection coefficients for turbulent flow of gases and liquids, GFSSP uses the Dittus-Boelter equation. For two-phase mixtures, GFSSP uses the Miropolskii correlation (1964). The Miropolskii correlation provides modified Nusselt, Reynolds, and Prandtl numbers based on fluid mixture parameter Y and mass fraction x where:

$$Y = 1 - 0.1\left(\left(\frac{\rho_l}{\rho_v} - 1\right)^{0.4}(1-x)^{0.4}\right) \tag{2}$$

$$Nu = 0.023\left(Re_{mix}\right)^{0.8}\left(Pr_v\right)^{0.4}\left(Y\right) \tag{3}$$

$$Re_{mix} = \left(\frac{\rho u D}{u_v}\right)\left(x + \left(\frac{\rho_v}{\rho_l}\right)(1-x)\right) \tag{4}$$

$$Pr_v = \left(\frac{C_p \mu_v}{k_v}\right) \tag{5}$$

To numerically model the system, the LH_2 transfer line assembly was broken up into nodes as shown in Figure 3. The nodal model consisted of a fluid flow network and a mass lump network. The model handles conjugate heat transfer as well as unsteady flow terms in the Navier-Stokes equations. Because the flow is routed vertically upward, the gravity term was also enabled. All frictional terms were also enabled, despite the low kinematic viscosity of cryogens. For the energy equation, the model includes solid and gas conduction, as well as radiation.

To model the system in GFSSP, it was first divided into four major subsections: the valve network at the inlet, the flow line downsteam of this network, the sight glass region, and the outflow network, as shown in Figure 3. The valve network was composed of 10 fluid nodes and 10 adjacent solid nodes, which each represented discrete sections of the tube network that connected a direct single path from the inlet valve to the valve at the flow line. The fluid and solid nodes were discretized in such a way to include specific lumps for the fittings and elbow mass concentrations as well as line pipe tube mass. The inlet boundary condition was set to match the experimental conditions. For the trickle flow cases, the mass flow rate was assigned by modifying the diameter of the orifice at Branch 1-2 until the desired flow rate was reached under a steady-state model. For the pulsed cases, the flow area for the Branch 1-2 was modulated using a ramp function with a ramp time of 0.125 s. For the initial solid nodes in this

section and all other sections, the temperature was set to best match the recorded initial temperatures of the temperature diodes with linearly interpreted values assigned to nodes between each measured location. The solid nodes were composed of stainless steel, with user-supplied temperature-dependent specific heat and thermal conduction files to accurately model properties down to cryogenic temperatures. Radiative heating from the environment was not included in this model.

Downstream of this section was the flow line, which was composed of 14 fluid and solid nodes. The lengths and masses for these nodes were equally divided with exceptions for the fittings at the edges of the line. The next section, modeled by the next 15 fluid and solid nodes, was the sight glass and sight glass cover mount region. The sight glass was modeled by 3 fluid nodes and 3 solid nodes composed of silica glass. The flexible bellows and sight glass protective canister were modeled with mass concentrations assigned to each of their respective nodes. The remaining nodes modelled the outflow network from the end of the sight glass cover mount to outside the vacuum chamber, then the 25-ft outflow line from the vacuum chamber to the outlet outside the facility. This outflow line was included to accurately incorporate the pressure gradient from the atmospheric boundary condition at the vent to the portion of the line located in the sight glass region.

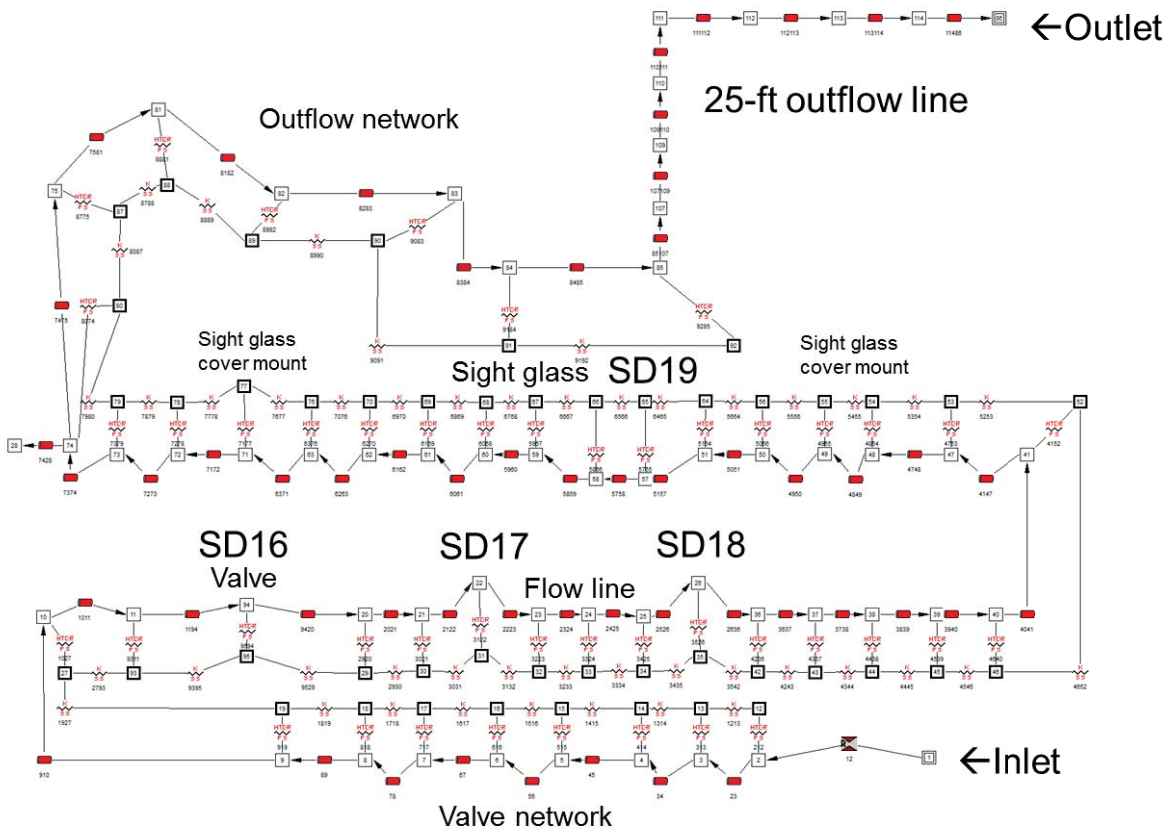

Figure 3: GFSSP Fluid Flow Network

To compare against the experimental data, 7 different cases were modeled across the parameter space of the data; these cases are shown in Table 1. Two different chilldown methods were examined, a trickle and a pulse flow method. Trickle flow is defined as a constant slow trickle of propellant through the line, less than 10% of the full steady state flow rate, with the line inlet and exit valves open for the duration of the process. It is the simplest method because it involves only a single valve opening. The second method is a pulse flow, where the line inlet valve is cycled and the line exit valve remains open, to allow LH_2 pulses into the transfer line at regular time intervals. The inlet valve duty cycle (DC) characterizes the pulse method, where DC is defined as:

$$DC = \frac{t_{open}}{t_{open} + t_{closed}} \tag{1}$$

For example, a 10/5 pulse has a DC of 0.667, where the inlet valve is cycled on for 10 seconds and off for 5 seconds, and repeated until steady state. The advantage of pulse flow is that it ensures complete liquid vaporization and likely uses the sensible and latent energy of the fluid more efficiently than trickle flow. The disadvantage is that success depends on valve cycling, rendering pulse flow more complex than trickle flow. Cases were run at several different inlet liquid saturation pressures, corresponding to 20.3K, 21.5K, 22.9K, and 24.2K saturation temperatures. The storage tank was pressurized with gaseous helium to subcool the liquid and suppress boiling as shown in column 4. Finally, the corresponding flow rate for medium and high flow legs at the different inlet liquid temperatures are included in Table 1. Variations in flow rate for a given method are due to higher driving pressures and lower kinematic viscosity at warmer temperatures relative to colder temperatures.

Case	Flow Description	Liquid Saturation Pressure [kPa]	Total Tank Pressure [kPa]	Flow Rate [kg/min]
1	Medium Trickle	103.42	206.84	0.69
2	High Trickle	103.42	206.84	1.59
3	Medium Trickle	137.90	206.84	0.66
4	Medium Trickle	206.84	275.79	0.86
5	Medium Trickle	275.79	344.74	1.01
6	10/5 Pulse	103.42	206.84	0.50
7	10/10 Pulse	103.42	206.84	0.38

Table 1: GFSSP Test Cases

Heaters were used to warm the line back to the initial starting temperature of 250K. However, the data shows that the initial conditions at the various skin mounted temperature sensors were non-uniform. Therefore, to match the data, the actual initial temperature at SD16 – 19 was directly fed into the model as shown in Table 2. Interpolation was used to determine the initial temperature at the nodes located between these diodes.

Case	SD-16 [K]	SD-17 [K]	SD-18 [K]	SD-19 [K]
1	234.4	248.7	355.5	277.1
2	219.9	225.9	241.2	261.4
3	220.1	235.0	244.9	261.7
4	245.6	244.4	246.3	264.1
5	245.4	244.2	246.9	265.1
6	230.2	251.1	338.3	270.4
7	245.5	243.9	245.4	263.7

Table 2: Initial Conditions at Various Skin Temperature Sensors

IV. Results, Discussion, and Comparison with the Data

Figure 4 plots the experimental data and the GFSSP predictions for the baseline case – medium trickle flow at 20.3K saturated liquid at the inlet. Examination of Figure 4a shows that all of the skin mounted temperature sensors quickly bottom out within the first 30 seconds of flow due to the high two phase flow boiling heat transfer between cold fluid and warm wall. The diodes mounted on the stainless steel (SS) tube portion of the assembly achieve LH_2 saturation temperatures quickly, while the diode mounted to the Pyrex bottoms out moments later. The three tube mounted temperature sensors bottom out in succession as the quenching front moves up the pipe as the system chills in. The skin diode mounted on the valve body (SD16) lags the pipe mounted diodes due to the additional mass of the

valve. Additional time is required to conductively cool portions of the valve body that lie outside the flow path. Eventually, the valve body does achieve steady state within 50 seconds.

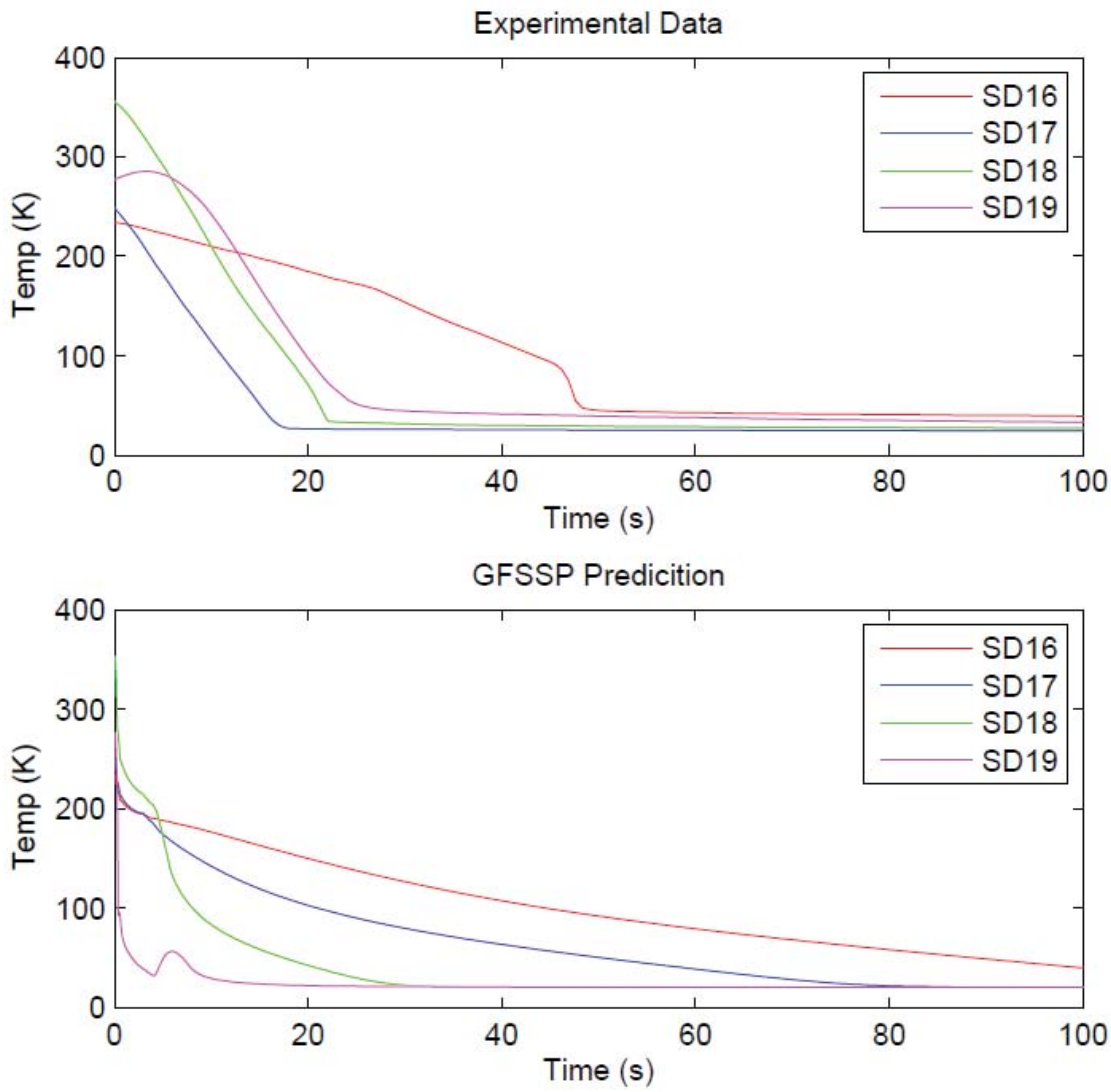

Figure 4: Comparison between a) Experimental Data and b) GFSSP Model Predictions for the Skin Mounted Temperature Sensors for the Medium Trickle Flow Chilldown Test at 20.3K Liquid Inlet Temperature

Figure 4b plots the corresponding model predicted curves for SD16 – 19. Comparison between Figures 4a and 4b shows that the model predicts a much smoother, slower transit time to steady state relative to the data. Qualitatively, the model tracks the trends in the data. The two SS mounted sensors agree well with the data. Data and model agree reasonably well for the valve mounted sensor as well. Data indicates that the cold fluid is able to remove thermal energy from the body much quicker than the model predicts. This discrepancy is due to transient flow velocity discrepancies, which would lead to significant error in modeling convection. The largest discrepancy between data and model is shown for the SG sensor. Discrepancies are likely due to the paucity of data for Pyrex properties at cryogenic temperatures, and due to the way the sight glass housing was modeled. Basic radiation calculations indicated that the housing material never achieved LH_2 temperatures even though the tube itself was at LH_2 temperatures, but the model shows that the entire assembly achieves steady state. The hump in the SD19 model curve is attributed to thermal feedback between warm valve body upstream and cold tube downstream. In general the model predicts less axial conduction and exhibits much smoother transitions to steady state than the data.

To examine the effect of varying the flow rate, Figures 5a and b plot data against GFSSP model predictions for the 20.3K high trickle flow case. Comparing Figures 4a to 5a, the data indicates that the system achieves steady state in less time, as anticipated; chilldown is achieved for all 4 diodes within 30 seconds. The model agrees better with data at the higher flow rate, apparently signifying a better Reynolds number regime for the application of GFSSP's Miropolski equation. The same characteristic hump is shown in the SG diode. At the higher flow rate, the model predicts that the valve mounted sensor achieves steady state faster than the data shows.

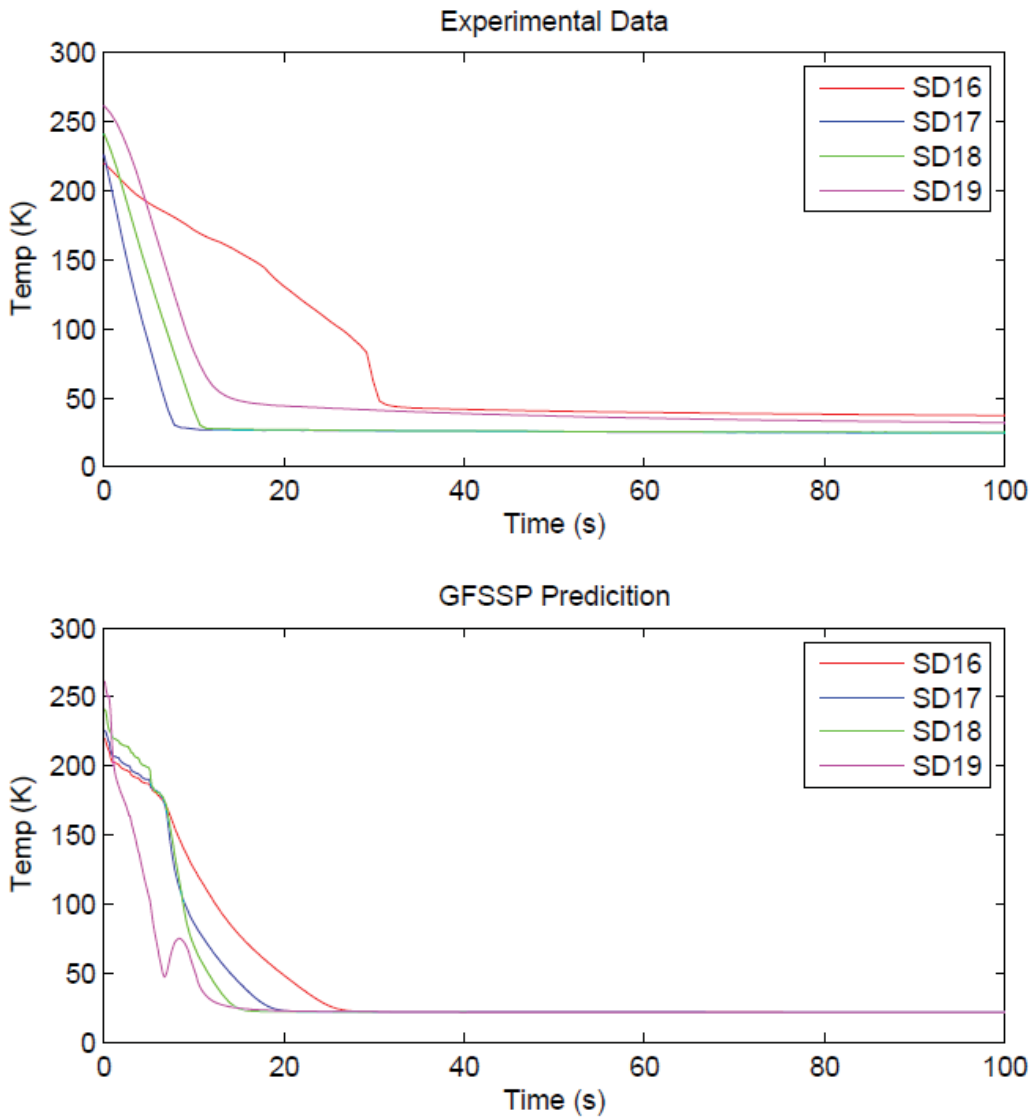

Figure 5: Comparison between a) Experimental Data and b) GFSSP Model Predictions for the Skin Mounted Temperature Sensors for the High Trickle Flow Chilldown Test at 20.3K Liquid Inlet Temperature

To examine the effect of varying the inlet liquid temperature, Figures 6a and b plot data and GFSSP model generated temperature traces for the 24.2K medium trickle flow case. Due to higher required driving pressures at elevated temperatures, and due to the reduced flow viscosity, data shows that chilldown is achieved in less time relative to the baseline 20.3K case. The model qualitatively tracks the trends again, with the greatest disparity again in the SG mounted sensor. The model again predicts that the SG achieves steady state before the SS mounted diodes. The model shows faster transitions to steady state at the warmer liquid temperature.

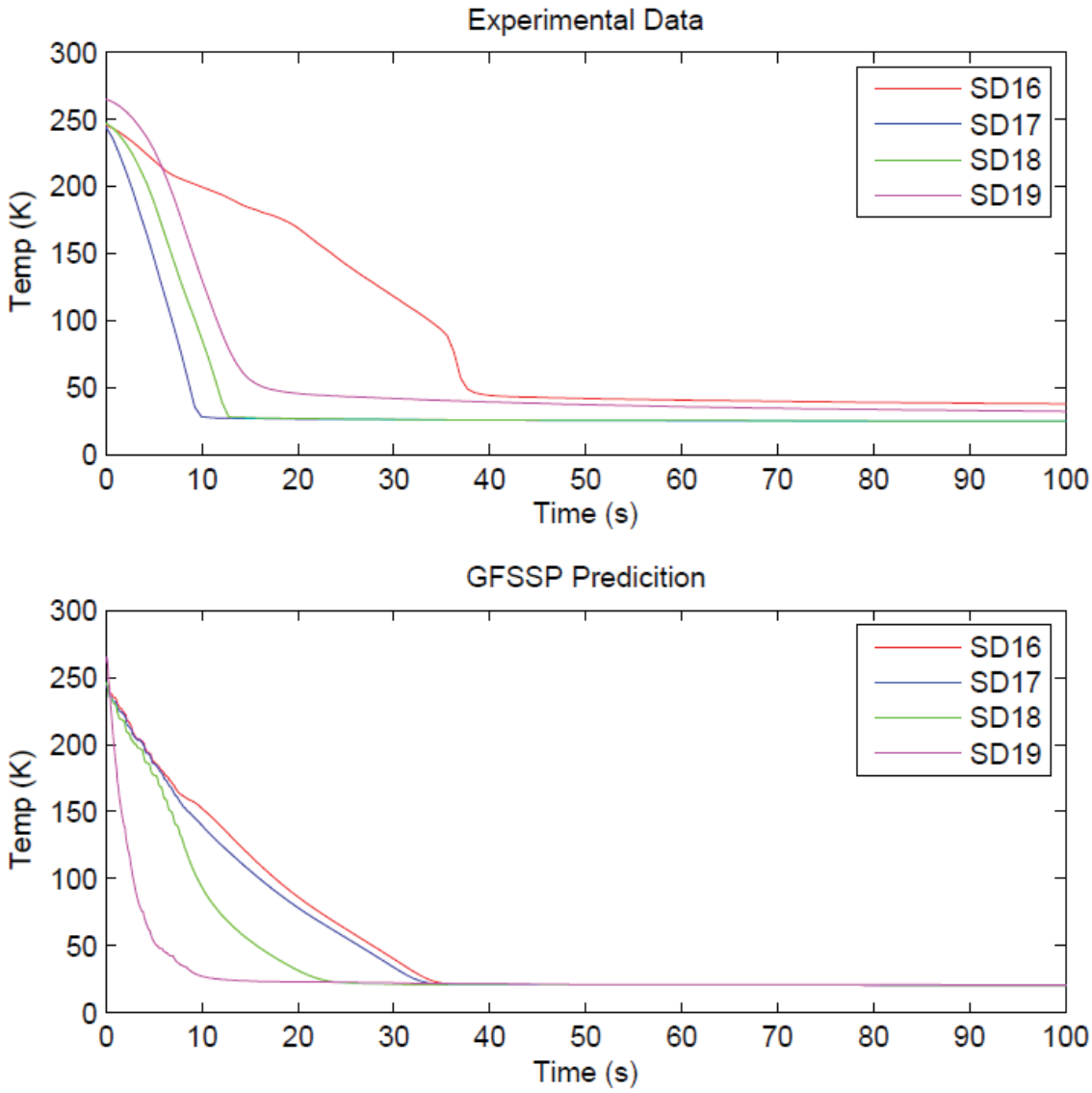

Figure 6: Comparison between a) Experimental Data and b) GFSSP Model Predictions for the Skin Mounted Temperature Sensors for the Medium Trickle Flow Chilldown Test at 24.2K Liquid Inlet Temperature

To examine the effect of varying the chilldown method, Figures 7a and b plot the data and model generated temperature traces for the 20.3K 10/5 pulse flow case. The same general behavior is shown in the temperature traces. All skin temperatures plummet quickly, but the final drop to steady state is prolonged relative to the medium trickle case. When the valve is on, the skin temperature drops; when the valve is cycled off, the skin temperature stabilizes. The valve body reading again lags the wall mounted readings. Comparing time to steady state, it is clear that trickle flows reach steady state faster than the 10/5 pulse case. The model qualitatively tracks the trends as shown in the data but the model generated traces are smoothed out relative to the data. The sensors mounted on the SS again achieve steady state after the SG Pyrex diode.

For the preceding cases, in general, the model predicts downstream locations chill down faster than upstream locations. This is likely due to the additional heat leak imposed by the sight glass can downstream that is not accounted for in the model. Second, the downstream vent pressure was held fixed, which partially imposes a condition upstream at the different pressure/temperature stations. Because the downstream locations are at lower pressures, the model computes lower saturation conditions locally and thus faster chilldown. Finally, the downstream temperatures may also be bottoming out earlier than the upstream locations due to the way the valves were modeled in GFSSP. Only

pipe nodes local to the valve nodes experience the effects of parasitic heat leak from the valves; these effects generally do not propagate to the downstream nodes.

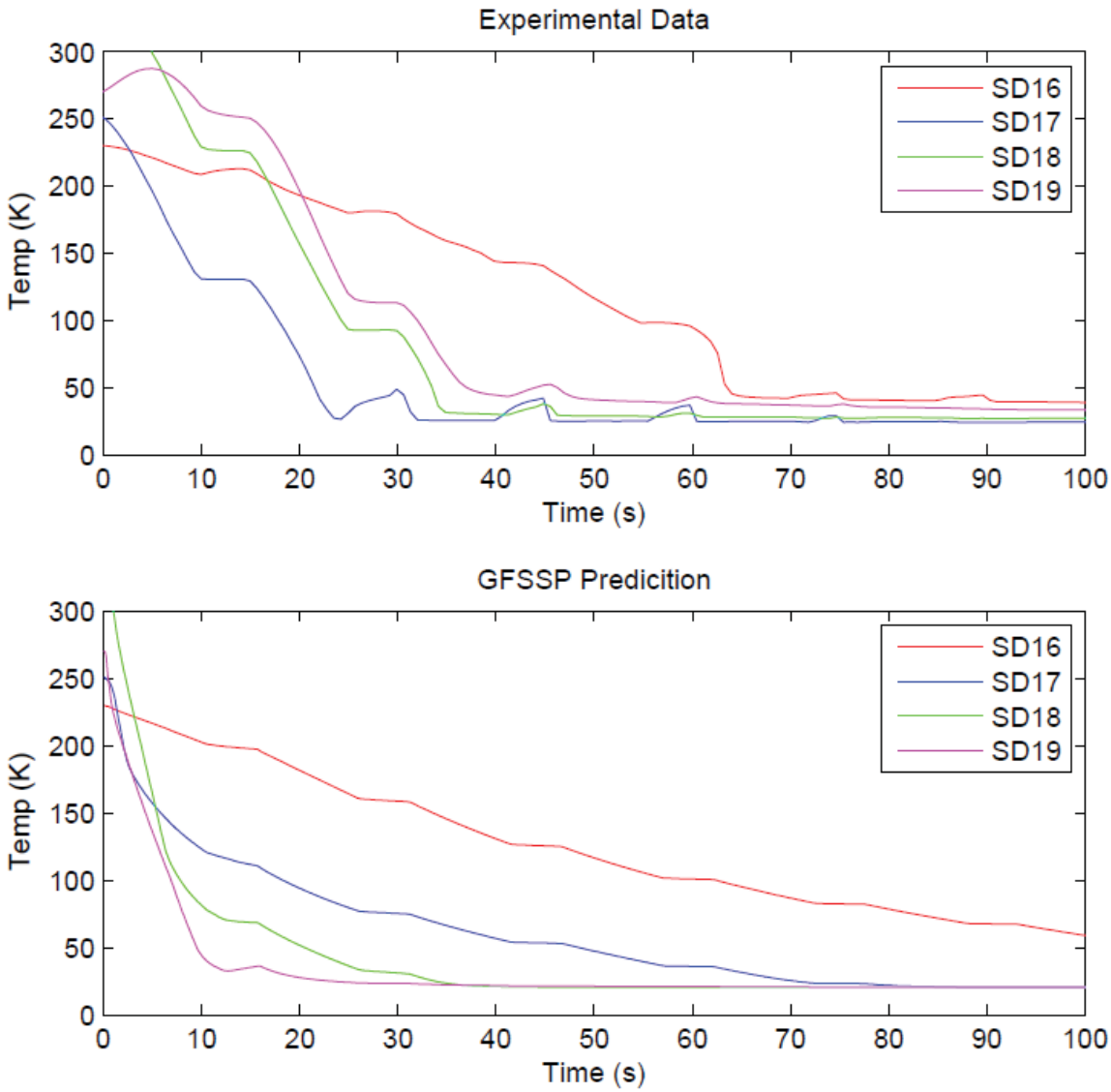

Figure 7: Comparison between a) Experimental Data and b) GFSSP Model Predictions for the Skin Mounted Temperature Sensors for the 10/5 Pulse Flow Chilldown Test at 20.3K Liquid Inlet Temperature

Figure 8 plots the actual vs. model generated internal stream temperature reading for the baseline 20.3K medium trickle flow case. As show, the measured stream temperature SD23 shows unexpected behavior. There are two points along the curve where the temperature actually increases, despite the line chill assembly being continually flooded with cold LH_2. This erratic behavior has been discussed previously, and is believed to be attributed to changes in the flow profiles. The stream diode was slightly recessed in a cross fitting directly downstream of the SG, and correlation of temperature traces with flow visualization from Rame et al. (2014) indicate that the two humps correspond to the vapor film to liquid droplet flow transition and annular to slug flow transitions seen in the SG. Eventually the stream temperature bottoms out and achieves steady state, corresponding to ultra-low quality bubbly flow. Flow visualization from Rame et al. (2014) confirms that the initial bottoming out of the skin diodes corresponds to annular flow, or a liquid film along the walls. Meanwhile the actual internal stream temperature does not achieve a steady state condition until much later, corresponding to a shift from annular to slug to churn to bubbly flow, and then to steady state vapor-free liquid. Clearly, there are profound discrepancies between wall mounted and internal mounted temperature measurements.

The model predicts that the stream temperature downstream of the SG bottoms out almost instantaneously. This is consistent with the SG skin sensor achieving steady state early. It appears that the model underpredicts the thermal feedback from the warm valve body upstream; data and flow visualization show that ultra-low quality flow is not achieved until long after the valve body reaches steady state.

Discrepancies between model and data are primarily due to the simplified GFSSP correlations used to predict two-phase heat transfer. Very little flow boiling data exist in the literature for cryogenic fluids, specifically LH_2. Flow visualization indicates that the system moves from vapor film boiling through dispersed droplet flow, annular flow, slug flow, churn flow, bubbly flow, and then single phase liquid flow. The same correlation is used in GFSSP to model heat transfer regardless of the flow regime.

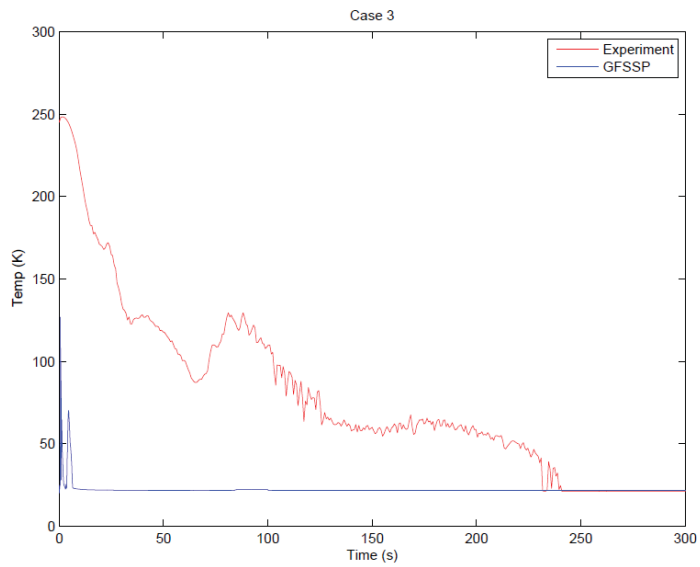

Figure 8: Comparison between Experimental Data and GFSSP Model Prediction of the Internal Stream Temperature Measurement for the Medium Trickle Chilldown Test at 20.3K Liquid Inlet Temperature

Discrepancies between data and model generated internal stream temperatures may also be due to high uncertainties in data from Brennan et al. (1966). To the author's knowledge, this is the first known internal mounted stream temperature for an LH_2 chilldown experiment; tests from Brennan et al. (1966) from which the GFSSP flow correlations were modeled, only incorporated skin temperature measurements. Those skin measurements were thermocouples, which have very low signal to noise ratio below liquid nitrogen temperatures. Therefore, data from Brennan et al. (1966) are suspect to scrutiny. Discrepancies may also be due to the difficulty in modeling a recessed temperature reading. Regardless of the source of discrepancy, experimental results here clearly warrant refinement to the manner in which GFSSP handles two phase flow, boiling, and heat transfer for liquid hydrogen.

V. Conclusion

A numerical model based on the GFSSP code was developed to model the transient chilldown process of a tank-to-tank cryogenic hydrogen propellant transfer line. Numerical results indicate that the model does well in tracking trends in the external skin mounted temperature readings across the trade space of chilldown methods, flow rates, and liquid inlet temperatures, with predictions better matching data at higher flow rates. The model predicts that skin temperatures downstream achieve steady state before sensors upstream due to a lack of data for Pyrex at cryogenic temperatures and due to underpredicting the effect of thermal feedback from the warm valve body upstream. Finally, very large discrepancies exist between data and model predicted internal fluid stream temperatures, and work is needed to refine the two-phase flow, boiling, and heat transfer correlations used within GFSSP for cryogenic propellant flow. Experimental work between the University of Florida and NASA is currently under way to gather data to re-optimize the two-phase heat transfer coefficient and critical heat flux within GFSSP, the results of which will be detailed in subsequent papers.

Acknowledgments

This work was funded by the Cryogenic Propellant Storage and Transfer Project under the Space Technology Mission Directorate at NASA.

References

[1]Chandler, F., Bienhoff, D., Cronick, J., and Grayson, G. "Propellant Depots for Earth Orbit and Lunar Exploration" *AIAA-2007-6081*, SPACE Conference, Long Beach, CA, September 18 – 20, 2007.

[2]Hartwig, J.W. "Liquid Acquisition Devices for Advanced In-Space Cryogenic Propulsion Systems" *Dissertation* Case Western Reserve University, May, 2014.

[3]Keefer, K. "Development and Validation of an Analytical Charge-Hold-Vent Model for Cryogenic Tank Chilldown" *Masters Thesis*, Case Western Reserve University, May, 2013.

[4]Taylor, W.J. and Chato, D.J. "Improved Thermodynamic Modeling of the No-Vent Fill Process and Correlation with Experimental Data" *AIAA-91-1379*, 26th Thermophysics Conference, Honolulu, HI, 1991.

[5]Wang, C.L., Wang, R.S., Li, Y., Xie, G.F., and Chang, C. "Comparison of the Performance About 4 Different Filling Configurations in No-Vent Fill Processes" *Cryogenics* 165, 35 – 39. 2008.

[6]Glahn, U.H. "A Correlation of Flim-Boiling Heat-Transfer Coefficients Obtained with Hydrogen, Nitrogen, and Freon 113 in Forced Flow" *NASA-TN-D-2294*, May 1, 1964.

[7]Kawanami, O., Azuma, H., and Ohta, H. "Effect of Gravity on Cryogenic Boiling Heat Transfer During Tube Quenching" *International Journal of Heat and Mass Transfer* 50, 3490 – 3497. 2007a.

[8]Kawanami, O., Nishida, T., Honda, I., Kawashima, Y., and Ohta, H. "Flow and Heat Transfer on Cryogenic Flow Boiling during Tube Quenching under Upward and Downward Flow" *Microgravity Science and Technology* 9.3 – 4, 137 – 138. 2007b.

[9]Hu, H., Chung, J.N., and Amber, S.H. "An Experimental Study on Flow Patterns and Heat Transfer Characteristics during Cryogenic Chilldown in a Vertical Pipe" *Cryogenics* 52, 268 – 277. 2012.

[10]Brennan, J.A., Brentari, E.G., Smith, R.V., and Steward, W.G. "An Experimental Report on Cooldown of Cryogenic Transfer Lines" *NBS Report 9264*, Boulder CO, November 7, 1966.

[11]Schuster, J.R., Howell, D.J., Lucas Jr., S.L., Haberbusch, M.S., Gaby, J.D., Van Dresar, N.T., and Wadel, M.F. "Cold Flow Testing of Revised Engine Chilldown Methods for the Atlas Centaur" *32nd AIAA-96-3014*, 32nd Joint Propulsion Conference, Lake Buena Vista, FL, July 1 – 3,1996.

[12]Rame, E., Hartwig, J.W., and McQuillen, J.B. "Flow Visualization of Liquid Hydrogen Line Chill Down Tests" *AIAA-2014-1074*, 2014 SciTech Conference, National Harbor, MD, January 13 – 17, 2014.

[13]Majumdar, A. and Van Hooser, K. "A Generalized Fluid System Simulation Program to Model Secondary Flows in Turbomachinery" *AIAA-95-2969*, 31st Joint Propulsion Conference, San Diego, CA, July 10 – 12, 1995.

[14]Schallhorn, P., Majumdar, A., Van Hooser, K., and Marsh, M. "Flow Simulation in Secondary Flow Passages of a Rocket Engine Turbopump" *AIAA-98-3684*, 34th Joint Propulsion Conference, Cleveland, OH, July 13 – 15, 1998.

[15]Richards, D. and Vonderwall, D. "Flow Network Analyses of Cryogenic Hydrogen Propellant Storage and Feed Systems" *AIAA-97-3098*, 33rd Joint Propulsion Conference, Seattle, WA, July 6 – 9, 1997.

[16]Majumdar, A. and Steadman, T. "Numerical Modeling of Pressurization of a Propellant Tank" *AIAA-99-0897*, 37th Aerospace Sciences Conference, Reno, NV, January 11 – 14, 1999.

[17]LeClair, A. and Majumdar, A. "Computational Model of the Chilldown and Propellant Loading of the Space Shuttle External Tank" 46th Joint Propulsion Conference, Nashville, TN, July 25 – 28, 2010.

[18]Majumdar, A. "No Vent Fill and Transfer Line Chilldown Analysis by Generalized Fluid System Simulation Program (GFSSP)" *2013 TFAWS Conference*, Daytona Beach, FL, July 29 – August 2, 2013.

[19]Sozen, M. and Majumdar, A. "A Novel Approach for Modeling Chemical Reaction in Generalized Fluid System Simulation Program" *AIAA-2003-4467*, 39th Joint Propulsion Conference, Huntsville, AL, July 20 – 23, 2003.

[20]Majumdar, A. "Numerical Modeling of Conjugate Heat Transfer in Fluid Network" 2004 TFAWS Conference, Pasadena, CA, August 30 – September 3, 2004.

[21]Miropolskii, Z. L., "Heat Transfer in Film Boiling of a Steam_Water Mixture in Steam Generating Tubes", Teploenergetika, Vol. 10, No.5, 1963, pp 49-52 (in Russian; translation Atomic Energy Commission, AEC-Tr-6252, 1964).